IEEE Access
Multidisciplinary | Rapid Review | Open Access Journal

Received 22 August 2023, accepted 1 November 2023, date of publication 16 November 2023,
date of current version 29 November 2023.

Digital Object Identifier 10.1109/ACCESS.2023.3334153

RESEARCH ARTICLE

A New Control Interaction Phenomenon in Large-Scale Type-4 Wind Park

LEI MENG[1], (Member, IEEE), ULAS KARAAGAC[1], (Member, IEEE), MOHSEN GHAFOURI[2], (Member, IEEE), ANTON STEPANOV[3], (Member, IEEE), JEAN MAHSEREDJIAN[3], (Fellow, IEEE), KA WING CHAN[1], (Member, IEEE), AND ILHAN KOCAR[1], (Senior Member, IEEE)

[1]Department of Electrical and Electronic Engineering, The Hong Kong Polytechnic University, Hong Kong
[2]Concordia Institute for Information Systems Engineering, Concordia University, Montreal, QC H3G 1M8, Canada
[3]Department of Electrical Engineering, Polytechnique Montréal, Montreal, QC H3T 1J4, Canada

Corresponding author: Ulas Karaagac (ulas.karaagac@polyu.edu.hk)

This work was supported in part by the Hong Kong Research Grant Council for the Research Project under Grant 25223118 and in part by the Hitachi-RTE MITACS Project.

ABSTRACT This paper demonstrates the risk of a new control interaction phenomenon between a large-scale type-4 wind park (WP) and a 500 kV transmission grid in a super-synchronous frequency range. This study aims at (i) using the impedance-based stability assessment (IBSA) method to investigate this new interaction phenomenon, (ii) analyzing the impact of various transmission grid topologies, WP operating conditions, and wind turbine (WT) converter control parameters on the severity of the interaction. For ultimate accuracy, the frequency-dependent impedance characteristics of the WP are extracted using the electromagnetic transient (EMT)-type impedance scanning instead of a simplified analytical model. The performed analyses demonstrate that the WP generation capacity, length of the transmission lines, applied series and shunt compensation levels, presence of parallel lines, and grid side converter (GSC) control parameters of the WT can significantly affect the identified instability risk. The obtained results are validated through detailed EMT simulations. Although the type-4 WP is considered in this paper, the presented results can be generalized to any inverter-based resource (IBR) with a full-size converter (FSC), such as photovoltaic (PV) power stations.

INDEX TERMS Control interaction, full-size converter, series compensation, shunt compensation, super-synchronous oscillation, transmission system, type-4 wind turbine.

I. INTRODUCTION

The penetration level of wind and solar energy and the size of their generation units have dramatically increased in the past decade. Recent incidents have shown that the photovoltaic (PV) inverters and grid side converter (GSC) of type-4 wind turbines (WTs) can adversely interact with the weakly tied AC grids at sub-synchronous frequency range [1]. This phenomenon is called weak grid sub-synchronous oscillation (SSO) [2].

In Texas, a type-4 wind park (WP) experienced weak grid SSO at 4 Hz in 2011 after one of the two parallel transmission lines connecting the WP to a strong grid was taken out of service [3]. In the Hami area of China, type-4 WPs experienced a weak grid SSO at 20 Hz in 2015 following an increase in WPs' output active power [4]. Large-scale WPs in the Hami area were connected to the main grid with long transmission lines, which created a weak grid condition. Other weak grid SSO events include 3.5 Hz oscillations in Hydro One's type-4 WPs in 2018 due to a planned bus outage and an increase in WP output active power [5]; 9 Hz oscillations in an offshore WP of Great Britain in 2019 [6]; 22 Hz oscillations in the PV power station of Dominion Energy in the eastern U.S. in 2021 due to an increase in PV output power [7]; and 7 Hz oscillations in First Solar's California PV power station in 2017 due to decrease in grid short circuit ratio (SCR) in some outage conditions [8].

The weak grid SSO mechanism was initially explained by circuit analysis as a power transfer problem [9]. When the reference value for the active power output of the grid

The associate editor coordinating the review of this manuscript and approving it for publication was Feiqi Deng.

inverter increases, the inverter output currents also increase. This leads to a more considerable voltage drop on equivalent grid impedance and decreases the inverter's active power output. The instability occurs due to the imbalance between the inverter output active power and the associated reference value. Based on this mechanism, a damping controller was designed to weaken the couplings between the inverter's active power and the voltage outputs [10]. The inverter controls also have significant impacts on the weak grid SSO. Initially, the phase-locked loop (PLL) parameters were found to be the major reason for the Texas and West China events, and modification of PLL parameters was recommended for mitigation [11]. Then, impedance-based stability analysis (IBSA) brings new insights into the weak grid SSO issue [4], [12]. The IBSA explains the instability as a circuit resonance formed by the grid inverter and the weak grid, and it can be displayed in the R-X diagram analysis [13], [14] or Bode diagram analysis [15]. The impacts of PLL, inner and outer control loops, decoupling, and voltage feedforward terms on the impedance characteristics of a grid inverter are analyzed in [12]. The weak grid SSO typically occurs when the inductive grid and capacitive inverter-based resource (IBR) impedances form a resonance with negative total resistance.

The IBSA method usage in IBR-related stability problems gained popularity due to its simplicity and computational effectiveness [12], [15]. Desired accuracy can be achieved when the frequency-dependent impedance model of the IBR is extracted using EMT-type impedance scanning instead of simplified analytical models. This method also allows extracting impedance characteristics of black-box or grey-box devices [13], [14], [16], [17].

This paper identifies a resonance condition between a large-scale type-4 WP and a 500 kV transmission grid in the super-synchronous frequency range. Transmission line charging capacitances, shunt, and series compensation levels play critical roles in the identified resonance. It should be emphasized that the weak grid SSO studies in the literature usually ignore the shunt branches (except the shunt harmonic filter of the grid inverter) as the external grid is typically represented with its Thevenin equivalent [9], [10], [11], [12]. The identified resonant frequency is in the super-synchronous range; hence, it is called super-synchronous oscillation (SupSO) in this paper. The detailed analysis demonstrates that transmission line length, applied series and shunt compensation levels, presence of parallel lines, WP generation capacity, and WT grid side converter (GSC) control parameters play important roles in the identified SupSO risk. The photovoltaic (PV) inverters and GSC of type-4 WTs have similar structures. Hence, the presented results and conclusions are also valid for PV solar plants. Based on the authors' knowledge, it is the first study in this regard.

The rest of this paper is arranged as follows. Section II briefly presents the type-4 WP model. The considered system and identified SupSO problem are introduced in Section III. Sections IV, V, and VI investigate the impact of the transmission grid, GSC control parameters, and WP operating conditions on SupSO, respectively. Section VII investigates the SupSO in lower voltage level systems. Section VIII provides simple mitigation guidelines. Finally, Section VIV concludes the paper.

II. TYPE-IV WIND TURBINE MODEL

The considered type-4 WT consists of a permanent magnet synchronous generator (PMSG) and a back-to-back converter. The converter system consists of two voltage source converters: a machine-side converter (MSC) and a GSC. A resistive chopper provides DC bus overvoltage protection. A line inductor (choke filter) and an AC shunt harmonic filter are used at the GSC end to improve the power quality. The type-4 WTs are connected to medium-voltage (MV) feeders through WT transformers, and these feeders form the MV collector grid that transfers the power from WTs to the point of interconnection (PoI) through a WP transformer.

Both MSC and GSC are controlled by two-level controllers. The slow outer control loop calculates the reference values for currents in dq-frame. The fast inner loop (current) controller, on the other hand, produces the converter voltage reference. MSC often operates at unity power factor and controls the active power through a maximum power point tracking (MPPT) algorithm. As its impact on the SupSO is negligible, this converter is not presented due to space limitations.

The simplified GSC control diagram is depicted in Fig. 1. The d- and q-axis currents of GSC (i_d and i_q) are used to control the DC bus voltage (V_{dc}) and positive sequence AC terminal voltage (V_{ac}), respectively. The primed variables indicate the reference values coming from controllers. The quantities in Fig. 1 and this section are per unit. The controller for AC voltage is a proportional (P) regulator, whose reference value (V'_{ac}=1 $+\Delta V'_{ac}$) is adjusted by the wind park controller (WPC) to achieve the desired reactive power level at the PoI. A typical setting for the AC voltage regulator is $K_V = 2$.

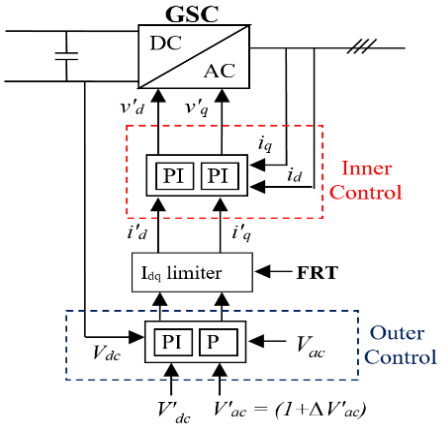

FIGURE 1. Simplified GSC control diagram [19].

The DC voltage controller is a proportional-integral (PI) regulator and is tuned based on inertia emulation, with

$$K_{p-dc} = \omega_0^2 \left(2H_{C-dc}\right) \ , \qquad K_{i-dc} = 2\xi\omega_0 \left(2H_{C-dc}\right) \quad (1)$$

where ω_0 is the natural frequency of the closed-loop system, and $\xi = 0.707$ is the damping factor; H_{C-dc} is the static moment of inertia, and it has

$$H_{C-dc} = E_{C-dc} \big/ S_{WT} \quad (2)$$

where E_{C-dc} is the stored energy in the DC bus capacitor (in Joules), S_{WT} is the WT rated power (in VA). K_{p-dc} and K_{i-dc} are calculated for the desired response time of a second-order system

$$\tau_{dc} = 3 \big/ \xi\omega_0 \quad (3)$$

The GSC controller gives priority to the active current during normal operation and the reactive current during severe voltage sag and swell conditions (fault-ride-through (FRT) operation) for grid-following operation.

The link between GSC output current and voltage can be described by a transfer function as

$$G\left(s\right) = 1 \big/ \left(R_\Sigma + sL_\Sigma\right) \quad (4)$$

where $Z_\Sigma = R_\Sigma + j\omega L_\Sigma$ represents the total series impedance between the aggregated GSC terminal and the external high voltage (HV) system Thevenin source. The parameters of inner current PI controllers are designed using the internal model control (IMC) method [18], [19],

$$K_{p-i} = \alpha_c L_\Sigma \ , \qquad K_{i-i} = \alpha_c R_\Sigma \quad (5)$$

where α_c is the set bandwidth. K_{p-i} and K_{i-i} can be calculated for the desired GSC rise time (t_{r-gsc}) using the relationship between a first-order system bandwidth and $10\% - 90\%$ rise time [18]

$$t_{r-gsc} = \ln\left(9\right) \big/ \alpha_c \quad (6)$$

Readers can refer to [19] for details of control parameter settings and EMT model of the considered type-4 WP. In EMT model, the MV collector grid and type-4 WTs are represented with their aggregated models, but the overall control structure of the WP is preserved. The type-4 WT and WP control system include the non-linearities, necessary transient and protection functions. Moreover, it allows the simulation of WPs' accurate transient behavior when they are subjected to external power system disturbances.

III. SYSTEM UNDER STUDY AND THE IDENTIFIED SUPER-SYNCHRONOUS OSCILLATION

A. THE SYSTEM UNDER STUDY

The system shown in Fig. 2 was originally developed based on a practical system and was used for investigating series capacitor sub-synchronous interaction (SSI) problems of type-3 WPs [13], [20]. The type-3 WTs are replaced with type-4 WTs in this research. The large-scale WP consists of 400 WTs and is connected to two large systems, i.e., System-1 and System-2, through Line-1 and Line-2. Line-1 is series compensated with 50% compensation level (CL) by two identical capacitor banks located at its ends. Two 230 MVAR identical shunt reactors are also installed at both ends of Line-1 to provide 75% total shunt compensation. Line-2 is short (100 km); thus, it does not contain any shunt or series compensation.

The converters are represented with their average value models (AVMs), and the simulation time step is 50 μs in all EMT simulations using EMTP [21]. Line-1 and Line-2 are represented with distributed constant parameter (CP) models. The wind park operates at rated wind speed and unity power factor.

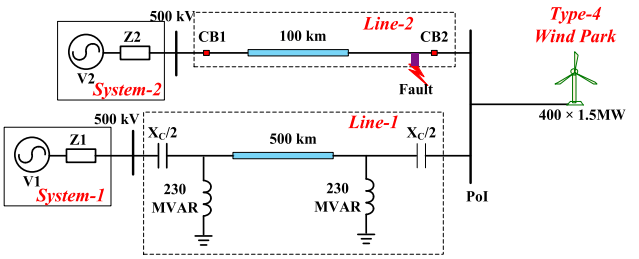

FIGURE 2. The system under study.

B. SUPER-SYNCHRONOUS OSCILLATION PHENOMENON

At $t = 4$ s (at perfect steady-state conditions), a single line-to-ground fault occurs in Line-2. It is cleared after 5 cycles by opening the circuit breakers (CB 1 and 2), leaving the wind park radially connected to System-1. It is seen in Fig. 3 that following this outage, a growing oscillation appears immediately in the WT output active and reactive power. Voltage and current fluctuations are found after fault clearance (in Fig. 4). The maximum GSC voltage exceeds its nominal value by 50% within 1 second. Both waveforms contain 21 Hz and 99 Hz components, which form a symmetrical pair around the synchronous frequency. The super-synchronous frequency component is larger compared to the sub-synchronous one, especially in voltage waveform.

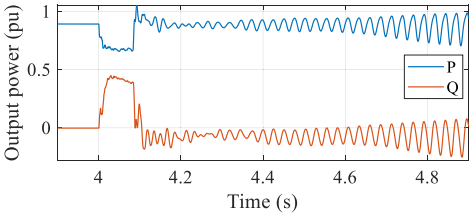

FIGURE 3. GSC active and reactive power outputs.

Since the SCR of this system is around 5 after Line-2 disconnection, this instability is not a typical weak grid issue. As illustrated in the following subsection, the resonance takes place at a super-synchronous frequency. The sub-synchronous frequency component appears due to the mirror frequency effect (MFE) [22]. It should be noted that when the SupSO occurs at a frequency larger than twice

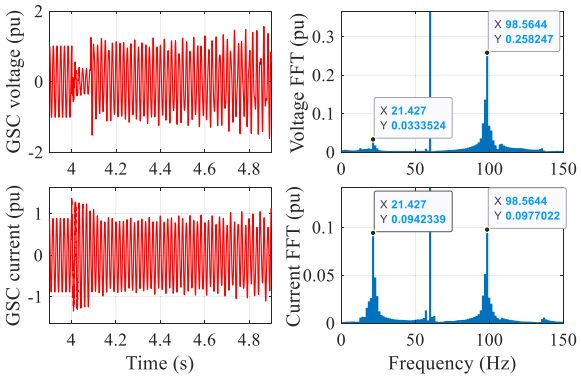

FIGURE 4. GSC voltage and current and their frequency spectra (phase-a).

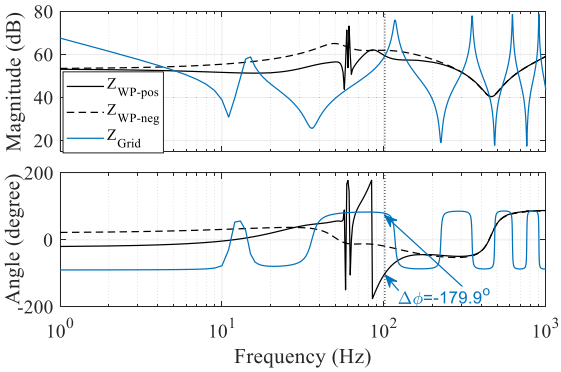

FIGURE 5. Impedance responses of the WP and transmission grid.

the fundamental frequency, its mirror coupling oscillation frequency becomes negative (i.e., the phase sequence of the oscillation is negative). As this research focuses on the SupSO risk after disconnection of Line-2, the following sections will only present the EMT simulation results of directly opening CBs at 4 second for simplicity.

C. INVESTIGATION OF THE SUPER-SYNCHRONOUS OSCILLATION

The 500 kV transmission grid frequency-dependent impedance is obtained using a phasor solution-based impedance scanning tool that is available in EMT simulators [23]. The WP frequency-dependent impedance is obtained through EMT-type impedance scanning using voltage sinusoidal perturbations with an amplitude of 0.02 pu. The frequency responses of the WP and transmission grid (when Line-2 is disconnected) for 1-1000 Hz frequency range are shown in Fig. 5. Z_{WP-pos} and Z_{WP-neg} are the WP impedances in positive and negative sequences, respectively. The grid side positive and negative sequence impedances are equivalent (Z_{Grid}).

As seen in Fig. 5, the transmission grid contains numerous parallel resonances generated by the transmission line charging capacitors and series inductors. These resonances may interact with WP at their intersection points, where $|Z_{WP}(f)| = |Z_{Grid}(f)|$, and lead to instability [24]. Stability at these intersections is assessed based on the Bode plot analysis criteria as presented in Table 1 [25].

For the intersection point at 101.5 Hz, the phase difference between grid and WP impedances ($\varphi_{Grid} - \varphi_{WP}$) is close to -180^o (-179.9^o). Such a small phase margin (PM), i.e., -0.1^o, indicates a critical unstable condition. Other intersection points are stable with large PMs regardless of the inductive or capacitive behavior of WP (or grid) as both the WP and grid have positive resistances. The frequencies of impedance interaction points are called crossover frequencies (f_C) in this paper. As seen in Fig. 5, the SupSO problem would be more severe if the parallel resonance of the grid shifted leftward or the WP had a smaller impedance magnitude.

Impact factors of both grid and WP side systems will be investigated in the following sections. As the system is safe from the negative sequence control interaction issue, only the positive sequence impedance-based analyses will be conducted in this paper. Although the usage of single-input single-output (SISO) positive sequence impedance model may lead to small discrepancies in the obtained resonance frequency and PM, these discrepancies can be neglected while analyzing parameter variations impact on system stability trend. Additionally, the positive sequence impedance gives insight into the impedance characteristics of WP and the instability mechanism.

TABLE 1. Bode plot analysis criteria at crossover frequency.

Rate of change of $\lvert Z_{Grid}(f_C)\rvert / \lvert Z_{WP}(f_C)\rvert > 0$	$\varphi_{Grid} - \varphi_{WP} > -180°$	Unstable
	$\varphi_{Grid} - \varphi_{WP} < -180°$	Stable
Rate of change of $\lvert Z_{Grid}(f_C)\rvert / \lvert Z_{WP}(f_C)\rvert < 0$	$\varphi_{Grid} - \varphi_{WP} > -180°$	Stable
	$\varphi_{Grid} - \varphi_{WP} < -180°$	Unstable

IV. IMPACT OF TRANSMISSION GRID ON THE SUPSO

This section investigates the impact of shunt and series CLs, compensation schemes, transmission line length, and the presence of parallel lines on the identified instability issue. The impact of different transmission line models on the identification of SupSO is also investigated.

A. TRANSMISSION LINE SERIES AND SHUNT COMPENSATION LEVELS

The considered variations in series and shunt CLs are presented in Table 2 with the associated IBSA results (i.e. crossover frequencies and PMs). As seen in Fig. 6, a decrease in either series or shunt CL increases the grid impedance magnitude ($|Z_{Grid}|$) and results in a decrease in f_C. As the change in grid impedance phase angle (φ_{Grid}) is marginal, the PM decreases significantly due to the variation in WP impedance phase angle (φ_{WP}), as seen in Fig. 6 and Table 2. EMT simulations in Fig. 7 confirm the IBSA results. In the considered 500 kV test system, smaller series and/or shunt CLs make the system more vulnerable to SupSO.

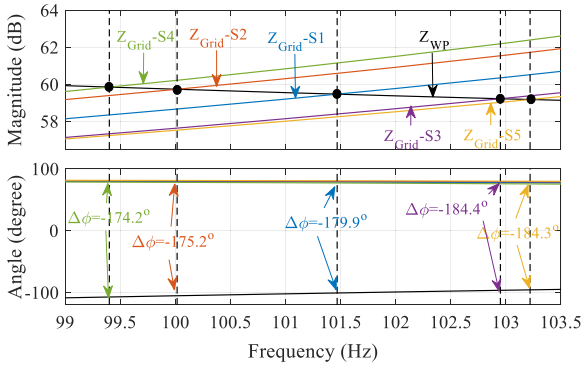

FIGURE 6. Impact of transmission line series and shunt CLs.

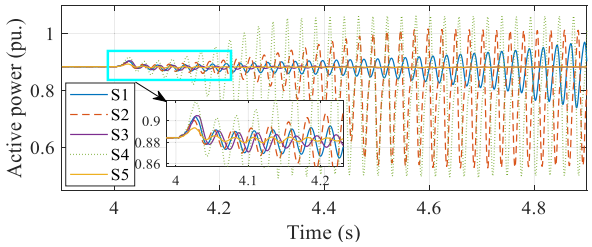

FIGURE 7. GSC active power outputs, scenarios S1-S5.

TABLE 2. Impact of transmission line compensation levels.

Scenario	S1	S2	S3	S4	S5
Series CL	50%	30%	70%	50%	50%
Shunt CL	75%	75%	75%	55%	95%
f_C (Hz)	101.5	100	103	99.4	103.2
PM	-0.1°	-4.8°	4.4°	-5.8°	4.3°

B. TRANSMISSION LINE LENGTH AND PRESENCE OF PARALLEL LINES

The IBSA results for different Line-1 lengths are presented in Table 3 and Fig. 8. The series and shunt CLs of Line-1 are modified considering its length to maintain the constant series inductance and charging capacitance levels. As seen in Fig. 8, the grid parallel resonance frequency increases significantly with the decrease in Line-1 length. Such an increase results in a larger f_C and PM as presented in Table 3. The SupSO risk is reduced when the WP is radially connected to System-1 with a shorter transmission line.

TABLE 3. Impact of transmission line length.

Scenario	Length	Series CL	Shunt CL	f_C	PM
S1	500km	50%	75%	101.5 Hz	-0.1°
S6	375km	33.3%	66.6%	111.9 Hz	21.6°
S7	250km	-	50%	132.5 Hz	42.9°

When the WP is connected to System-1 via identical parallel lines, the shunt resonance frequency of the grid decreases significantly (see Fig. 9) as the increase in equivalent shunt charging capacitance is more significant compared to the decrease in equivalent series inductance. The

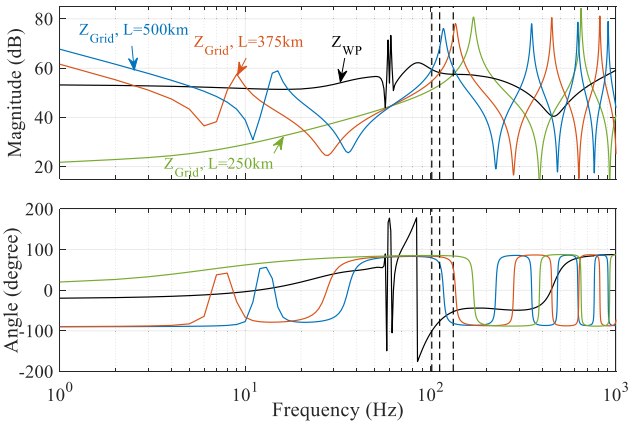

FIGURE 8. Impact of transmission line length (see Table 3 for f_C and PM).

presence of parallel lines increase the SupSO risk rather than reducing it as seen in Table 4.

TABLE 4. Impact of parallel transmission lines.

Line	500km 2-lines	500km 3-lines	375km 2-lines	375km 3-lines	250km 2-lines	250km 3-lines
f_C (Hz)	93.0	85.6	101.5	92.8	116.0	104.3
PM	-17.4°	-39.2°	6.0°	-30.6°	31.7°	15.1°

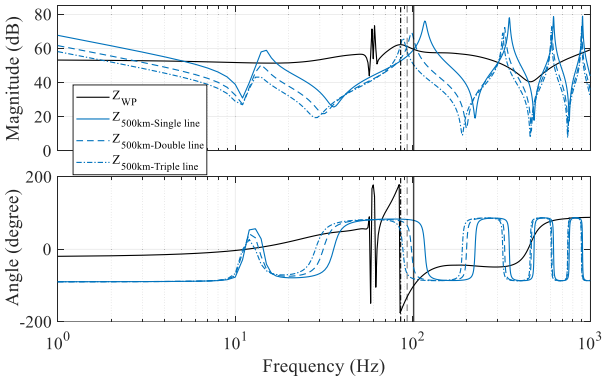

FIGURE 9. Impact of parallel transmission lines (see Table 4 for f_C and PM).

C. SERIES AND SHUNT COMPENSATION SCHEMES

Some of the typical transmission line shunt and series compensation schemes are presented in Table 5, and their impedance characteristics are shown in Fig. 10 (a). It can be learned that the compensation schemes affect the equivalent grid impedance characteristics Z_{Grid} (f) mainly at low frequency range. Hence, its impact on the SupSO instability is marginal. The IBSA results in Table 6 and EMT simulations in Fig. 10 (b) confirm this observation. On the other hand, usage of simplified transmission line models, namely, representing the distributed CP line model by a PI-equivalent circuit or a series RLC branch (defined as configurations d and e, respectively) has significant impact on the IBSA result.

TABLE 5. Series and shunt compensation schemes of transmission line.

No.	Configuration	No.	Configuration
(a)	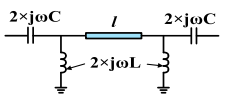	(b)	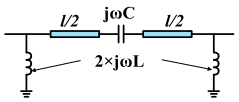
(c)	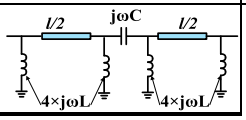		

Usage of PI-equivalent and series RLC representations mainly changes the impedance characteristics of the transmission line from middle to high frequency range (from one hundred to thousands of Hz). As shown in Table 6, the accuracy of using the PI-equivalent model can be considered as acceptable, whereas using the series RLC branch fails to capture the instability as expected. As the line charging capacitances and shunt compensation inductors play important roles on the identified SupSO, it is inappropriate to simply classify this problem as a weak grid instability.

TABLE 6. Impact of compensation schemes and transmission line models.

Configuration	*a*	*b*	*c*	*d*	*e*
f_C (Hz)	101.5	99.4	99.8	100.2	182.9
PM	-0.1°	-0.4°	-0.2°	-5.0°	47.9°

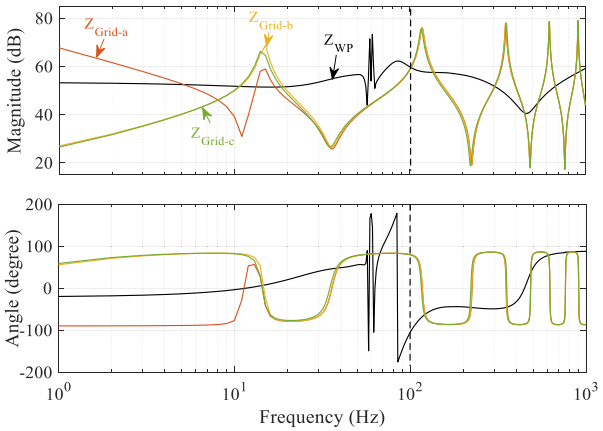

(a) $Z_{Grid}(f)$ (configurations a - c) and $Z_{WP}(f)$, see Table VI for f_C and PM.

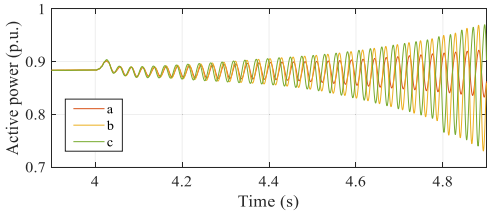

(b) GSC active power outputs (for configurations a - c)

FIGURE 10. Impact of transmission line series and shunt compensation schemes.

V. IMPACT OF GSC CONTROL ON THE SUPSO

A. GSC INNER CONTROL LOOP PARAMETERS

The GSC inner current control loop rise time t_{r-gsc} (see (6)) in S1 is 6 ms and is modified within its typical setting range (2.5 to 10 ms). The length variations of Line-1 given in Table 3 are also considered. Definitions of the considered scenarios and corresponding IBSA results are presented in Table 7 and Table 8.

TABLE 7. Scenarios for illustrating gsc rise time impact.

Length \ t_{r-gsc}	10 (ms)	7.5 (ms)	5 (ms)	2.5 (ms)
500 (km)	S8	S9	S10	S11
375 (km)	S12	S13	S14	S15
250 (km)	S16	S17	S18	S19

TABLE 8. Crossover frequency and phase margin of S8-S19.

Scenario	S8	S9	S10	S11
f_C (Hz)	101.4	101.2	101.9	103.5
PM	54.9°	23.7°	-17°	-58°
Scenario	S12	S13	S14	S15
f_C (Hz)	114.4	112.5	112	114.9
PM	66.3°	45.4°	5.6°	-35.1°
Scenario	S16	S17	S18	S19
f_C (Hz)	140.3	135.8	130.7	132.2
PM	68.7°	56.8°	29.5°	-12.6°

Decreasing t_{r-gsc} significantly reduces WP resistance value in the frequency range of interest (see Fig. 11), thereby reducing the system PM. For $t_{r-gsc} = 2.5$ ms, all considered scenarios become unstable. In scenario 19 (250 km transmission line), the crossover frequency even exceeds the double fundamental frequency, and the mirror coupling component in this scenario is a negative sequence signal of 12.2 Hz. For $t_{r-gsc} = 7.5$ ms and above, all scenarios of the considered transmission line variations are stable. The EMT simulations presented in Fig. 12 confirm the IBSA results in Table 8.

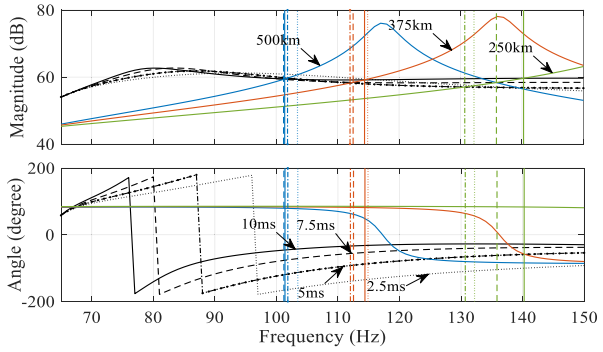

FIGURE 11. Impact of GSC rise time (see Table 8 for f_C and PM).

B. GSC OUTER CONTROL LOOP PARAMETERS

1) DC VOLTAGE REGULATOR PARAMETERS

The DC voltage regulator parameters affect the frequency response of GSC especially at 60 Hz - 120 Hz frequency

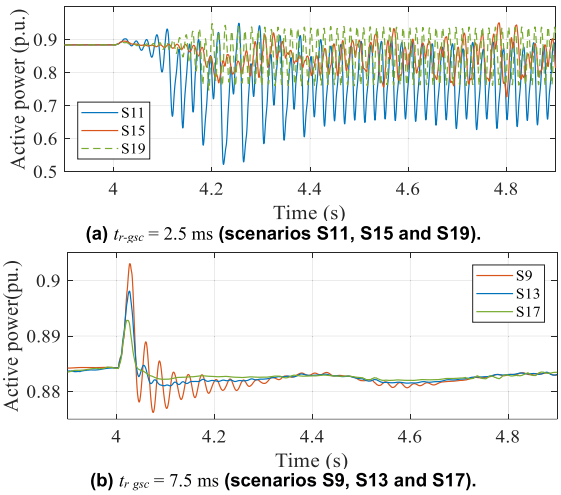

(a) $t_{r\text{-}gsc}$ = 2.5 ms **(scenarios S11, S15 and S19).**

(b) $t_{r\ gsc}$ = 7.5 ms **(scenarios S9, S13 and S17).**

FIGURE 12. GSC active power outputs for different t_{r-gsc}.

range as seen from Fig. 13 (a). Similar to the GSC current regulator, decreasing the DC voltage regulator response time (τ_{dc}) reduces the WP resistance. This results in a decrease in system PM as well (see Table 9). However, its impact is much smaller compared to the GSC current regulator parameters. The EMT simulation results shown in Fig. 13 (b) confirm the presented IBSA results in Table 9.

TABLE 9. Impact of WT GSC dc-voltage regulator time constant.

Scenario	S20	S1	S21	S22
τ_{dc} (ms)	75	150	250	400
f_C (Hz)	100.8	101.5	101.8	101.9
PM	-15.5°	-0.1°	4.8°	7.2°

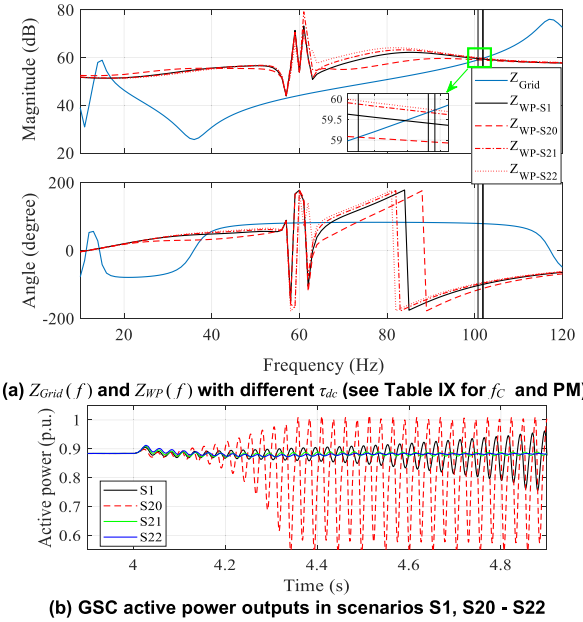

(a) $Z_{Grid}(f)$ **and** $Z_{WP}(f)$ **with different** τ_{dc} **(see Table IX for** f_C **and PM).**

(b) GSC active power outputs in scenarios S1, S20 - S22

FIGURE 13. Impact of DC voltage regulator response time.

2) AC VOLTAGE REGULATOR GAIN

Increasing the AC voltage regulator gain (K_V) decreases the WP resistance significantly as seen from Fig. 14, and results in a significant decrease in PM of the system (see Table 10). The EMT simulation results shown in Fig. 15 confirm the IBSA results.

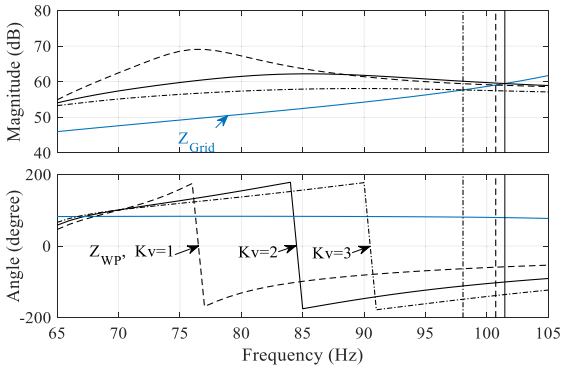

FIGURE 14. Impact of GSC AC voltage regulator gain (f_C and PM Table 10).

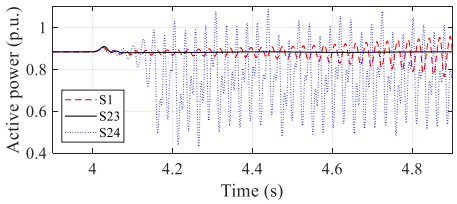

FIGURE 15. GSC active power outputs in scenarios S1, S23, and S24.

TABLE 10. Impact of GSC AC voltage regulator parameter.

Scenario	S23	S1	S24
K_V	1	2	3
f_C (Hz)	100.7	101.5	98.1
PM	40.9°	-0.1°	-49.8°

According to new German grid code [19], the AC voltage regulator gain setting range should be $2 \leq K_V < 6$. Usage of large K_V values may make the system very vulnerable to the SupSO even for large GSC rise time settings.

VI. IMPACT OF WP OPERATING CONDITIONS ON THE SUPSO

A. WT OUTAGES AND WP INSTALLED CAPACITY

The number of installed and in-service WTs in the WP (N_i and N_S, respectively) are given in Table 11. As seen in Fig. 16(a), with the increase of WT outages, the impedance magnitude of WP increases almost proportionally, while the phase angle remains almost unchanged in the super-synchronous range. This leads the interaction point of the system shifting to larger frequency where the WP has larger resistance. The WP becomes less vulnerable to the SupSO when more WTs are out of service. EMT simulations shown in Fig. 16(b) confirm the IBSA results. If the installed capacity was

smaller, we would observe again larger WP impedance due to reduced number of WTs (even more compared to WT outage scenarios due to decreased size of WP transformer). Larger size WP is expected to be more vulnerable to the SupSO.

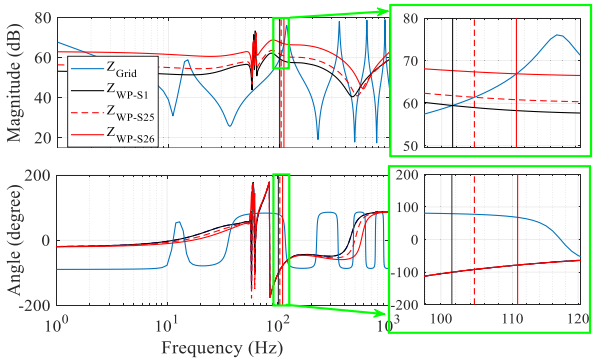

(a) $Z_{Grid}(f)$ and $Z_{WP}(f)$ (see Table XI for f_C and PM).

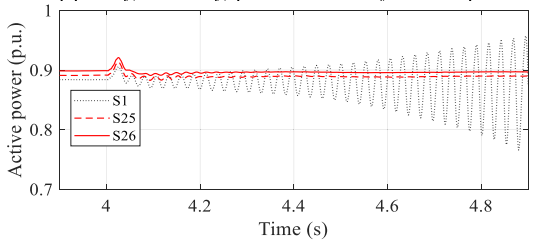

(b) GSC active power outputs in scenarios S1, S25 and S26

FIGURE 16. Impact of WT outages.

TABLE 11. Impact of WT outage and the number of installed WTs.

Scenario	S1	S25	S26
N_i	400	400	400
N_S	400	300	200
f_C (Hz)	101.5	104.6	110.7
PM	-0.1°	10.4°	33.6°

B. IMPACT OF WP ACTIVE AND REACTIVE POWER GENERATION

The impact of WP reactive power generation and wind speed (i.e., WP active power generation) are marginal as presented in Table 12 and Table 13. The increase in either reactive power generation or wind speed slightly increases the stability margin. The IBSA results are confirmed with EMT simulations shown in Fig. 17.

TABLE 12. Impact of WP reactive power.

Scenario	S27	S28	S1	S29	S30
Q (pu)	-0.2	-0.1	0	0.1	0.2
f_C (Hz)	101.1	101.3	101.5	101.7	101.9
PM	-3.8°	-2.1°	-0.1°	1.0°	2.5°

VII. SUPSO RISKS IN DIFFERENT VOLTAGE LEVEL SYSTEMS

The SupSO risks are investigated in three similar systems in different voltage levels (i.e., 400, 315 and 230 kV).

TABLE 13. Impact of wind speed.

Scenario	S1	S31	S32
WS (pu)	1	0.8	0.6
f_C (Hz)	101.5	100.8	100.2
PM	-0.1°	-2.4°	-3.2°

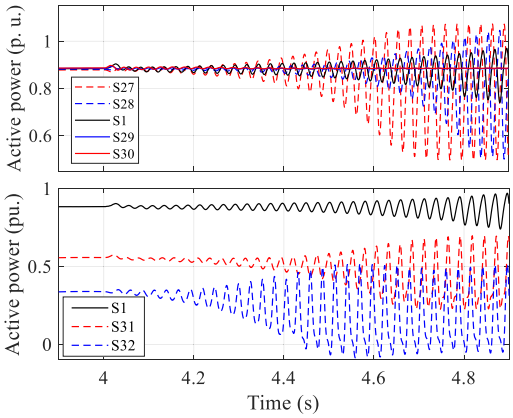

FIGURE 17. GSC active power outputs in scenarios S1, S27 - S32.

Transmission line parameters of these systems come from practical systems and are presented in Table 14. The WP capacity, transmission line length and compensation levels are adjusted considering the power transmission capability in different voltage levels.

TABLE 14. Parameters of systems with different voltage levels.

V-Level	Line Len.	Line Param.	Series CL	Shunt CL	N_S
400 kV	375 km	R= 0.0209 Ω/km X_L=0.3192 Ω/km X_C=5.1949 μS/km	50%	66.7%	350
315 kV	275 km	R= 0.0289 Ω/km X_L=0.3640 Ω/km X_C=4.5372 μS/km	50%	\	250
230 kV	150 km	R= 0.0575 Ω/km X_L=0.4800 Ω/km X_C=3.4352 μS/km	33.3%	\	200

Note: R, X_L, and X_C are resistance, inductive reactance, and charging capacitance of transmission line (per km).

It is seen in Fig. 18 and Table 15 that type-4 WPs integrated to lower voltage level power grids are also vulnerable to the SupSO. The instability risk would be higher if the GSC inner loop response speed is high. It should be noted that with the decrease in voltage level, the resonance frequency of the SupSO increases significantly and exceeds the double fundamental frequency. EMT simulations in Fig. 19 confirm the IBSA results.

VIII. GUIDELINES FOR SUPSO MITIGATION

According to the investigations conducted in the previous sections, the potential SupSO problem is expected to be more severe at full WT in-service, long transmission line length, low series and shunt CLs, and parallel lines conditions.

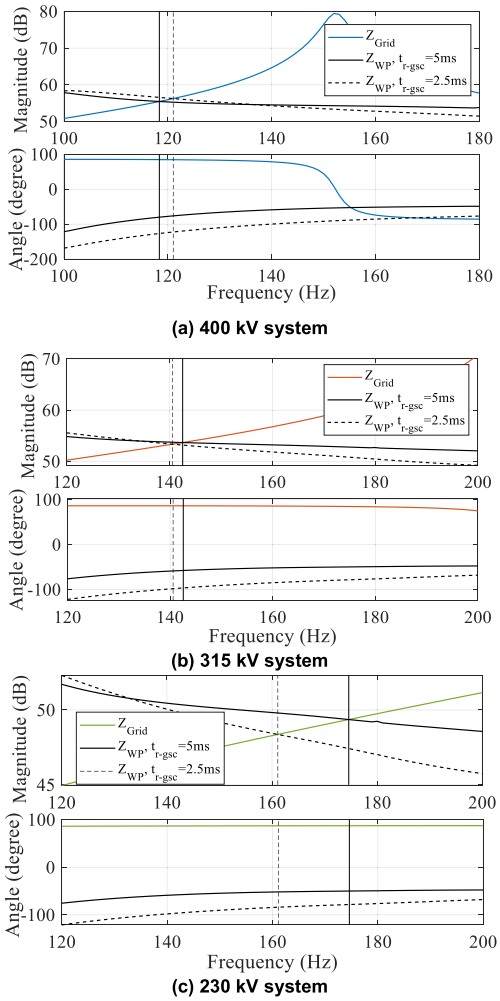

FIGURE 18. Impact of GSC rise time in different voltage level systems (see Table 15 for f_C and PM).

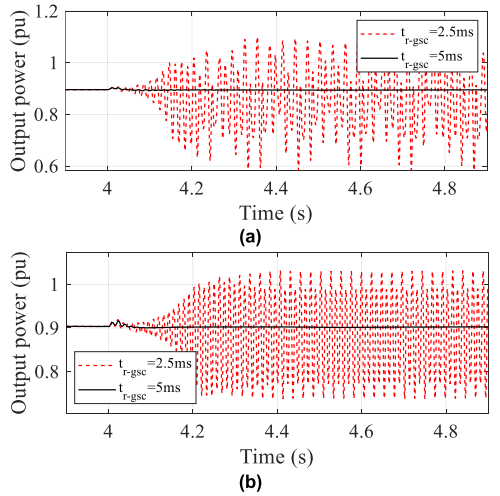

FIGURE 19. GSC active power outputs (a) 400 kV and (b) 315 kV systems.

Hence, a scenario (S33) considering these extreme operating conditions is generated to study the SupSO mitigation (see Table 16). As demonstrated in Section V, the GSC inner control loop rise time and AC voltage regulator gain have significant impact on the SupSO performance. Thus, this paper recommends when a SupSO risk is detected, increasing the inner control loop rise time for mitigation (S34 in Table 16).

TABLE 15. Impact of GSC rise time in different voltage levels.

V-Level	$t_{r\text{-}gsc}$	f_C (Hz)	PM
400 kV	5 ms	118.4	15.3°
	2.5 ms	121.0	-26.8°
315 kV	5 ms	142.6	36.3°
	2.5 ms	140.6	-4.4°
230 kV	5 ms	174.6	42.8°
	2.5 ms	161.1	9.0°

The system PM would be extremely low if the 3-lines model is adopted in S33. Under this condition, the t_{r-gsc} value is required to be increased significantly, which may exceed its normal setting range and decrease the GSC inner control loop response speed. To compensate for the sluggish inner loop response and maintain an acceptable transient response, the voltage regulator gain can be slightly increased. It is worth noting that, although transmission system operators (TSOs) usually suppress the series capacitor associated oscillations by bypassing one or more capacitor banks in transmission grid. This strategy is ineffective in the identified SupSO phenomenon. Bypassing capacitors even reduces PM of the system (see S35 in Table 16).

TABLE 16. The proposed SupSO mitigation scenarios and strategies.

Scen -ario	Line	Series CL	Shunt CL	$t_{r\text{-}gsc}$	f_C (Hz)	PM
S33	500km 2-lines	30%	55%	5ms	89.4	-51.8°
S34	500km 2-lines	30%	55%	10ms	89.0	27.8°
S35	500km 2-lines	30% and 0	55%	5ms	88.5	-56.8

IX. CONCLUSION

This paper identified a SupSO phenomenon for a large-scale type-4 WP radially connected to 500 kV grid through a long transmission line. The grid side impedance contains several parallel and series resonances formed by the transmission line charging capacitances and series inductances. The parallel resonance that interacts with the WP in 60-180 Hz frequency range causes instability where the negative resistance of the WP has a larger magnitude compared to grid positive resistance. As both the grid and WP have positive resistances at other frequency ranges, instability is not expected.

The parallel resonance frequency of the transmission grid is significantly affected by the line length and applied shunt and series compensation levels. For the considered 500 kV test system, the SupSO risk is more severe for a longer

transmission line with lower shunt and series compensation levels. Additionally, presence of parallel lines significantly increases the instability risk. To identify the potential SupSO risk, the transmission lines should be represented at least with their PI-equivalent models.

The WP is more vulnerable to the SupSO while operating with the slowest wind speed and largest possible capacitive reactive power generation. However, the WP operating condition has a marginal impact compared to the WT GSC control parameters. GSC with either a fast inner loop response speed or a large AC voltage regulator gain induces high SupSO risk. The SupSO risk in a smaller-scale WP (with smaller installed capacity or WT outages) is smaller. Type-IV WP integrated to a lower voltage level power grid can also be vulnerable to the SupSO risk if the WT GSC response speed is high.

When a SupSO risk is detected, the response speed of the inner control loop and/or the ac voltage regulator gain can be reduced for mitigation as long as an acceptable transient response to voltage sags and swells is maintained.

As the PV inverters and GSC of type-4 WTs have similar structures, the presented results and drawn conclusions are also valid for PV solar plants.

REFERENCES

[1] Y. Cheng, L. Fan, J. Rose, S.-H. Huang, J. Schmall, X. Wang, X. Xie, J. Shair, J. R. Ramamurthy, N. Modi, C. Li, C. Wang, S. Shah, B. Pal, Z. Miao, A. Isaacs, J. Mahseredjian, and J. Zhou, "Real-world subsynchronous oscillation events in power grids with high penetrations of inverter-based resources," *IEEE Trans. Power Syst.*, vol. 38, no. 1, pp. 316–330, Jan. 2023.

[2] *Wind Energy Systems Sub-Synchronous Oscillations: Events and Modeling*, document PES-TR80, AMPS Committee, IEEE-PES Wind SSO Task Force, Jul. 2020.

[3] S.-H. Huang, J. Schmall, J. Conto, J. Adams, Y. Zhang, and C. Carter, "Voltage control challenges on weak grids with high penetration of wind generation: ERCOT experience," in *Proc. IEEE Power Energy Soc. Gen. Meeting*, Jul. 2012, pp. 1–7.

[4] H. Liu, X. Xie, J. He, T. Xu, Z. Yu, C. Wang, and C. Zhang, "Subsynchronous interaction between direct-drive PMSG based wind farms and weak AC networks," *IEEE Trans. Power Syst.*, vol. 32, no. 6, pp. 4708–4720, Nov. 2017.

[5] C. Li and R. Reinmuller, "Asset condition anomaly detections by using power quality data analytics," in *Proc. IEEE Power Energy Soc. Gen. Meeting (PESGM)*, Aug. 2019, pp. 1–5.

[6] *Technical Report on the Events of 9 August 2019*, National Grid ESO, London, U.K., 2019.

[7] *Identifying Oscillations Injected by Inverter-Based Solar Energy Sources in Dominion Energy's Service Territory Using Synchrophasor Data and Point-on-Wave Data*, Dominion Energy, Richmond, VA, USA, Apr. 2021.

[8] *Deploying Utility-Scale PV Power Plants in Weak Grids*, First Solar, Tempe, AZ, USA, Jun. 2017.

[9] L. Fan and Z. Miao, "An explanation of oscillations due to wind power plants weak grid interconnection," *IEEE Trans. Sustain. Energy*, vol. 9, no. 1, pp. 488–490, Jan. 2018.

[10] Y. Li, L. Fan, and Z. Miao, "Stability control for wind in weak grids," *IEEE Trans. Sustain. Energy*, vol. 10, no. 4, pp. 2094–2103, Oct. 2019.

[11] L. Fan and Z. Miao, "Wind in weak grids: 4 Hz or 30 Hz oscillations," *IEEE Trans. Power Syst.*, vol. 33, no. 5, pp. 5803–5804, Sep. 2018.

[12] H. Liu and X. Xie, "Comparative studies on the impedance models of VSC-based renewable generators for SSI stability analysis," *IEEE Trans. Energy Convers.*, vol. 34, no. 3, pp. 1442–1453, Sep. 2019.

[13] U. Karaagac, J. Mahseredjian, S. Jensen, R. Gagnon, M. Fecteau, and I. Kocar, "Safe operation of DFIG-based wind parks in series-compensated systems," *IEEE Trans. Power Del.*, vol. 33, no. 2, pp. 709–718, Apr. 2018.

[14] Y. Cheng, M. Sahni, D. Muthumuni, and B. Badrzadeh, "Reactance scan crossover-based approach for investigating SSCI concerns for DFIG-based wind turbines," *IEEE Trans. Power Del.*, vol. 28, no. 2, pp. 742–751, Apr. 2013.

[15] J. Sun, "Impedance-based stability criterion for grid-connected inverters," *IEEE Trans. Power Electron.*, vol. 26, no. 11, pp. 3075–3078, Nov. 2011.

[16] B. Badrzadeh, M. Sahni, Y. Zhou, D. Muthumuni, and A. Gole, "General methodology for analysis of sub-synchronous interaction in wind power plants," *IEEE Trans. Power Syst.*, vol. 28, no. 2, pp. 1858–1869, May 2013.

[17] A. S. Trevisan, Â. Mendonça, R. Gagnon, J. Mahseredjian, and M. Fecteau, "Analytically validated SSCI assessment technique for wind parks in series compensated grids," *IEEE Trans. Power Syst.*, vol. 36, no. 1, pp. 39–48, Jan. 2021.

[18] L. Harnefors and H.-P. Nee, "Model-based current control of AC machines using the internal model control method," *IEEE Trans. Ind. Appl.*, vol. 34, no. 1, pp. 133–141, Jan. 1998.

[19] U. Karaagac, J. Mahseredjian, R. Gagnon, H. Gras, H. Saad, L. Cai, I. Kocar, A. Haddadi, E. Farantatos, S. Bu, K. Chan, and L. Wang, "A generic EMT-type simulation model for wind parks with permanent magnet synchronous generator full size converter wind turbines," *IEEE Power Energy Technol. Syst. J.*, vol. 6, no. 3, pp. 131–141, Sep. 2019.

[20] M. Ghafouri, U. Karaagac, J. Mahseredjian, and H. Karimi, "SSCI damping controller design for series-compensated DFIG-based wind parks considering implementation challenges," *IEEE Trans. Power Syst.*, vol. 34, no. 4, pp. 2644–2653, Jul. 2019.

[21] J. Mahseredjian, S. Dennetière, L. Dubé, B. Khodabakhchian, and L. Gérin-Lajoie, "On a new approach for the simulation of transients in power systems," *Electr. Power Syst. Res.*, vol. 77, no. 11, pp. 1514–1520, Sep. 2007.

[22] A. Rygg, M. Molinas, C. Zhang, and X. Cai, "A modified sequence-domain impedance definition and its equivalence to the dq-domain impedance definition for the stability analysis of AC power electronic systems," *IEEE J. Emerg. Sel. Topics Power Electron.*, vol. 4, no. 4, pp. 1383–1396, Dec. 2016.

[23] IEEE Subsynchronous Resonance Working Group, "Reader's guide to subsynchronous resonance," *IEEE Trans. Power Syst.*, vol. 7, no. 1, pp. 150–157, Feb. 1992.

[24] M. Céspedes and J. Sun, "Modeling and mitigation of harmonic resonance between wind turbines and the grid," in *Proc. IEEE Energy Convers. Congr. Expo.*, Phoenix, AZ, USA, Sep. 2011, pp. 2109–2116.

[25] Y. Liao and X. Wang, "General rules of using Bode plots for impedance-based stability analysis," in *Proc. IEEE 19th Workshop Control Modeling Power Electron. (COMPEL)*, Jun. 2018, pp. 1–6.

LEI MENG (Member, IEEE) received the B.Sc. degree in control theory and control technology and the M.Sc. degree in electrical engineering from Northeastern University, China, in 2016 and 2019, respectively. She is currently pursuing the Ph.D. degree with the Department of Electrical and Electronic Engineering, The Hong Kong Polytechnic University, Hong Kong, SAR, China. Her research interests include the control interaction issues between inverter-based resources and transmission grid, and EMT-type impedance scanning methods.

ULAS KARAAGAC (Member, IEEE) received the B.Sc. and M.Sc. degrees in electrical and electronics engineering from Middle East Technical University, Ankara, Turkey, in 1999 and 2002, respectively, and the Ph.D. degree in electrical engineering from Polytechnique Montréal, Montreal, QC, Canada, in 2011. He was a Research and Development Engineer with the Information Technology and Electronics Research Institute (BILTEN), Scientific and Technical Research Council of Turkey (TUBITAK), from 1999 to 2007. He was also a Postdoctoral Fellow with Polytechnique Montréal, from 2011 to 2013, and a Research Associate, from 2013 to 2016. In 2017, he joined the Department of Electrical Engineering, The Hong Kong Polytechnic University, as a Research Assistant Professor. His research interests include the integration of large-scale renewables into power grids, the modeling and simulation of large-scale power systems, and power system dynamics and control.

MOHSEN GHAFOURI (Member, IEEE) received the B.Sc. and master's degrees in electrical engineering from the Sharif University of Technology, Tehran, Iran, in 2009 and 2011, respectively, and the Ph.D. degree in electrical engineering from Polytechnique Montréal, Montreal, QC, Canada, in 2018. He was a Researcher with the Iranian Power System Research Institute, Sharif University of Technology, from 2011 to 2014. In 2018, he was a Researcher with CYME International, Eaton Power System Solutions, Montreal. In August 2018, he joined as a Horizon Postdoctoral Fellow with the Security Research Group, Concordia University, where he is currently an Assistant Professor. His research interests include the cybersecurity of smart grids, power system modeling, microgrid, wind energy, and the control of industrial processes.

ANTON STEPANOV (Member, IEEE) received the Engineering degree in electrical and power systems from South Ural State University, Chelyabinsk, Russia, in 2013, the M.Sc. degree in electronic systems and electrical engineering from Ecole Polytechnique de l'Université de Nantes, Saint-Nazaire, France, in 2015, and the Ph.D. degree in electrical engineering from Polytechnique Montréal, Montreal, QC, Canada, in 2020. From 2017 to 2020, he was a recipient of the Vanier Canada Graduate Scholarship. In 2020, he joined PGSTech, Canada, as a Research and Development Specialist. His research interests include HVDC systems modeling, analysis, and simulation.

JEAN MAHSEREDJIAN (Fellow, IEEE) received the M.A.Sc. and Ph.D. degrees from Polytechnique Montréal, Montreal, QC, Canada, in 1985 and 1991, respectively. From 1987 to 2004, he was with IREQ (Hydro-Quebec), working on research and development activities related to the simulation and analysis of electromagnetic transients. In December 2004, he joined the Faculty of Electrical Engineering, Polytechnique Montréal, where he is currently a Professor.

KA WING CHAN (Member, IEEE) received the B.Sc. (Hons.) and Ph.D. degrees in electronic and electrical engineering from the University of Bath, Bath, U.K., in 1988 and 1992, respectively. He is currently an Associate Professor and the Associate Head of the Department of Electrical Engineering, The Hong Kong Polytechnic University, Hong Kong. His general research interests include power system stability, analysis and control, power grid integration, security, resilience and optimization, and demand response management.

ILHAN KOCAR (Senior Member, IEEE) received the B.Sc. and M.Sc. degrees in EEE from Orta Doğu Teknik Üniversitesi, Ankara, Turkey, in 1998 and 2003, respectively, and the Ph.D. degree in EE from École Polytechnique de Montréal (affiliated with Université de Montréal), Montreal, QC, Canada, in 2009. He is currently a Professor with The Hong Kong Polytechnic University, Hong Kong. He has 20 years of experience with career highlights in research, development of computational tools for power system analysis, project engineering, and consulting. He is an Associate Editor of IEEE TRANSACTIONS ON POWER DELIVERY and *Journal of Modern Power Systems and Clean Energy*.